Research Square

Preprints are preliminary reports that have not undergone peer review.
They should not be considered conclusive, used to inform clinical practice,
or referenced by the media as validated information.

Development of W-Modified FeMnNiCoCr High-Entropy Alloy by Wire Arc Additive Manufacturing

Anatoliy Zavdoveev

avzavdoveev@gmail.com

E.O.Paton Electric Welding Institute https://orcid.org/0000-0003-2811-0765

Dmytro Vedel
Ji Junwen
Nikša Čatipović
Mykola Skoryk
Andrej Klapatyuk
Sviatoslav Motrunich
Valeriy Pozniakov
Viacheslav Kopylov
Massimo Rogante
Iaroslav Lavrenko

Research Article

Keywords: Fe-rich high-entropy alloy, tungsten microalloying, wire arc additive manufacturing, metal powder cored wire, microstructure evolution, solid-solution strengthening, additive manufacturing, mechanical properties, refractory element

Posted Date: July 17th, 2026

DOI: https://doi.org/10.21203/rs.3.rs-10059400/v1

License: This work is licensed under a Creative Commons Attribution 4.0 International License.
Read Full License

Development of W-Modified FeMnNiCoCr High-Entropy Alloy by Wire Arc Additive Manufacturing

Anatoliy Zavdoveev[1,2*], Dmytro Vedel[3], Ji Junwen[4], Nikša Čatipović[5], Mykola Skoryk[6], Andrej Klapatyuk[1], Sviatoslav Motrunich[1], Valeriy Pozniakov[1], Viacheslav Kopylov[3], Massimo Rogante[7], Iaroslav Lavrenko[8]

[1] *E.O. Paton Institute of Electric Welding Paton NAS of Ukraine, K. Malevicha 11, 03150, Kyiv, Ukraine*

[2] *Donetsk Institute of Physics and Technology named after O.O. Galkina NAS of Ukraine, Nauky Ave., 46, Kyiv, 03028, Ukraine*

[3]*. Institute of Problems of Materials Science named after I.M. Frantsevich of the National Academy of Sciences of Ukraine 3 Omelyan Pritsak (Krzhyzhanovsky) St., Kyiv, 03142*

[4] *E.O. Paton Educational and Scientific Institute of Materials Science and Welding of the National Technical University of Ukraine "Igor Sikorsky Kyiv Polytechnic Institute" (NN IMZ named after E.O. Paton), 35 Polytechnic St., 03056, Kyiv, Ukraine.*

[5]*Faculty of Electrical Engineering, Mechanical Engineering and Naval Architecture, University of Split, 21000 Split, Croatia*

[6] G.V. Kurdyumov Institute of metal physics NAS of Ukraine, Kyiv Ukraine

[7]*Rogante Engineering Office, Contrada San Michele 61, 62012 Civitanova Marche, Italy*

[8]*Department of Dynamics and Strength of Machine and Strength of Materials, National Technical University of Ukraine "Ihor Sikorsky Kyiv Polytechnic Institute", Kyiv, Ukraine Prospect Beresteiskyi (former Peremohy) 37,*

Corresponding author: avzavdoveev@gmail.com, +380973482383

Abstract

A tungsten modified Fe-rich Cantor-type high-entropy alloy was fabricated by wire arc additive manufacturing using a metal powder cored wire feedstock. Thermodynamic calculations predicted the formation of a stable solid-solution structure without pronounced secondary phase precipitation, while differential scanning calorimetry revealed multi-stage crystallization associated with the refractory nature of W. X-ray diffraction analysis confirmed the formation of a single BCC solid-solution phase after deposition, indicating effective dissolution of W within the alloy matrix. The deposited walls exhibited elongated columnar grains with pronounced microstructural variation along the build direction due to differences in local cooling conditions

during WAAM processing. SEM-EDS analysis demonstrated a homogeneous distribution of alloying elements without visible macrosegregation. The obtained results demonstrate that W addition effectively modifies the structural state and mechanical response of Fe-rich Cantor-type HEAs and confirms the potential of metal powder cored wire technology for the development of compositionally complex alloys for large-scale additive manufacturing applications.

Key words: Fe-rich high-entropy alloy; tungsten microalloying; wire arc additive manufacturing; metal powder cored wire; microstructure evolution; solid-solution strengthening; additive manufacturing; mechanical properties; refractory element;

1. Introduction

High-entropy alloys (HEAs) have significant scientific and industrial attention due to their unique combination of mechanical properties, thermal stability, and corrosion resistance [1–4]. In contrast to conventional alloys based on one principal element, HEAs consist of multiple elements components mixed in near-equiatomic concentrations. It promotes the formation of simple solid-solution phases stabilized by high configurational entropy [1]. Among the various HEA systems, the equiatomic Cantor alloy ($Fe_{0.2}Mn_{0.2}Ni_{0.2}Co_{0.2}Cr_{0.2}$) is considered one of the most extensively investigated compositions due to it high ductility, fracture toughness, and structural stability in a wide temperature range [5]. These properties make Cantor-type alloys promising candidates for advanced engineering applications operating under extreme loading and thermal conditions.

The additive manufacturing technologies to produce high-entropy alloys one of the most discussed topics [2,6–8]. Additive manufacturing enables the fabrication of components with reduced material consumption, high deposition efficiency, and flexible control of chemical composition and geometry. The wire arc additive manufacturing (WAAM) is one of the most promising methods for large-scale metallic components due to its high deposition rate, low equipment cost, and high material utilization efficiency [9–16]. In comparison with powder-bed

technologies, WAAM provides a significantly higher productivity, which is particularly important for structural applications and large-sized parts. Despite these advantages, the WAAM processing of high-entropy alloys remains challenging. The fabrication of compositionally complex HEAs using conventional solid wires is technologically limited due to difficulties associated with alloy preparation and wire production. Therefore, the development of alternative feedstock approaches for WAAM of HEAs is an important scientific and technological task[17–19].

One promising solution is the application of metal powder cored wire, which enables flexible adjustment of alloy composition through the controlled filling of elemental powders into a metallic sheath. This approach significantly simplifies the fabrication of compositionally complex alloys and provides the possibility of introducing refractory elements into the system. In particular, tungsten is of considerable interest due to its high melting temperature, high hardness, and strong solid-solution strengthening effect [17,19]. The addition of tungsten (W) into Cantor-type HEAs can potentially improve physical and mechanical properties. Therefore, understanding the phase formation and microstructure evolution of W-containing HEAs produced by WAAM is essential. In the present work, a W-containing FeMnNiCoCr high-entropy alloy was fabricated by wire arc additive manufacturing using a metal powder cored wire feedstock. The phase composition, microstructure evolution, elemental distribution, and tensile properties of the deposited alloy were systematically investigated. Special attention was devoted to the dissolution behavior of tungsten in the Cantor alloy matrix and its influence on the structural homogeneity and mechanical response of the WAAM-fabricated material.

2. Materials and methods

2.1. Metal powder cored wire (MPCW) manufacturing

For the production of the MPCW feedstock material used in this work, an ultra-low carbon steel (C 0.05, Si 0.05, Mn 0.35, Ni ≤ 0.30, S ≤ 0.04, P ≤ 0.035, Fe balance, wt.%) stripe with a size of 0.4 × 10 mm was used [17]. The filling coefficient was set at 60%. The steel strip was placed into

forming rolls and eventually the raw powders were added onto the surface of the steel after which enveloping rolls were used to create the wire-shaped feedstock composed of an outer layer of the steel strip and within by the raw powder mixing Ni, Mn, Cr, Co and W. After the enveloping stage, wire drawing until a final diameter of 2.4 mm was obtained was implemented. Here, it should be mentioned that multiple drawing steps were performed to avoid diameter reductions above 23 % . Hence, the MPCW wire drawing route was performed as follows: Φ = 3.8 to 3.4, 3.0,2.75 and finally to 2.4 mm (with associated partial reductions of 20, 22, 16 and 23%, respectively). The average composition of the wire core was determined to be 24,75% Cr, 24,75% Mn, 24,75% Co, 24,75% Ni, 1%W wt%. A schematic representation of the MPCW feedstock is detailed in figure 1.

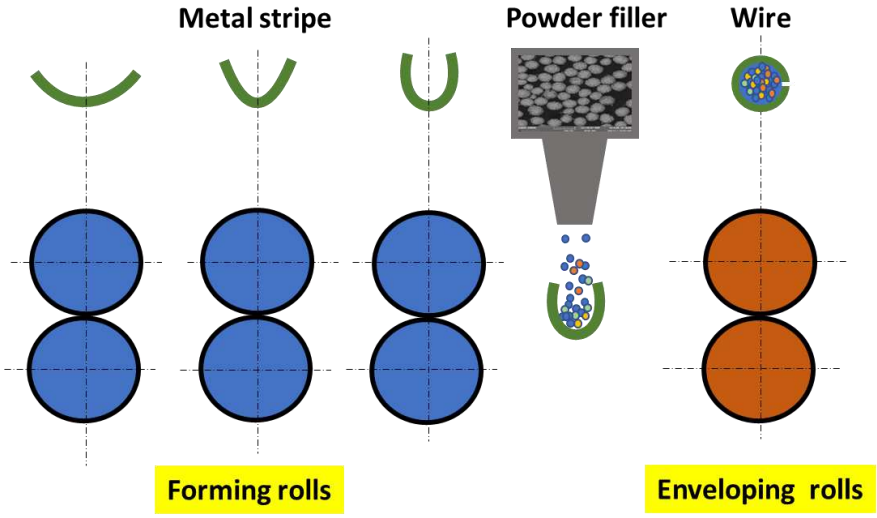


Figure 1. Schematic representation of the MPCW feedstock material used for WAAM in this work.

A VDU-506 power supply was used for melting and deposit the MPCW feedstock material. The deposition parameters metal deposition, the deposition conditions included a current ranging from 280 to 350A and an arc voltage between 32 and 34V. The depositions of each layer were performed with the previously deposited layer was between 200 and 250□C. To achieve stable deposition conditions the wire feed speed was varied between 77 and 90 mm/s.

A WAAM all with a total of ten layers was deposited. The monolithic sample measured 150x35x20 mm. The deposition was made on the high strength low alloy steel substrate with a width 50 mm and thickness of 14 mm.

2.1 Material characterization

An X-ray diffractometer Rigaku Ultima IV (Japan), with CuKα radiation, step size 2θ=0.02◦, and acquisition time τ =2 s was used to identify the crystalline phases in the wall

The microstructure of the wall and cross section of the wall was analyzed using a scanning electron microscope, MIRA 3 (Tescan Co., Czech Republic). The chemical composition was measured using an energy dispersive X-ray microanalyzer Oxford X-Max 80 with an active crystal area of 80 mm^2 (INCA X-Max, Oxford Instruments, Abingdon-on- Thames, UK). The local chemical composition was performed with an acceleration voltage of 10 kV. The exposure time for chemical analysis was 30 s. Indexing of the Energy-dispersive X-ray spectrum was carried out through the commercial software INCA (Oxford Instruments, Abingdon-on-Thames, UK).

The tests were performed on the universal servo-hydraulic test set MTS 318.25 with a maximum force of 250 kN. This complex ensures rigid loading of the sample, which is especially relevant when determining the modulus of elasticity and yield strength. Control of parameters during tests was carried out using the standard software TestWorks 4 of the MTS 318.25 system. This specialized licensed software makes it possible to monitor the selected parameters of the experiment in real time and to receive in electronic format the values of the standard characteristics describing the behavior of the material during the deformation process. The tests were carried out in a rigid mode with a loading speed in accordance with ISO 6892-1:2019 standart. The load speed was controlled by the movement of the active gripper of the testing machine. For a more accurate determination of the conventional yield strength of the base metal, the speed of movement of the gripper on the linear section of the "stress-strain" diagram and in the zone of elastic-plastic deformation was 2 mm/min. The measurement accuracy was 0.001

mm, the measurement base was 30 mm. In the future, the rate of loading until the sample broke was 10 mm/min.

Thermodynamic calculations were performed using Thermo-Calc software employing the TCHEA thermodynamic database. The equilibrium phase stability and non-equilibrium solidification behavior of the investigated alloy were evaluated based on the experimentally determined chemical composition. Equilibrium calculations were carried out using the Equilibrium Calculator module to predict the phase constitution as a function of temperature. The solidification path was simulated using the Scheil–Gulliver model, assuming complete mixing in the liquid phase and negligible diffusion in the solid state. The calculations were performed over the temperature range from 1600 to 25 °C.

3. Results and discussion

The raw powders had the angular shape for Cr, Mn and spherical shape for Ni, Co, and W **Fig. 2**. The average particle size was in the range of 100 - 150 μm for Ni, Mn and Cr, respectively **Fig. 2 b, d. c.** While, the particle size for Co and W was 10-20 μm. The small particle size of the tungsten was chosen to have uniform distribution throughout the entire volume in the core-wire, **Fig. 2 g**.

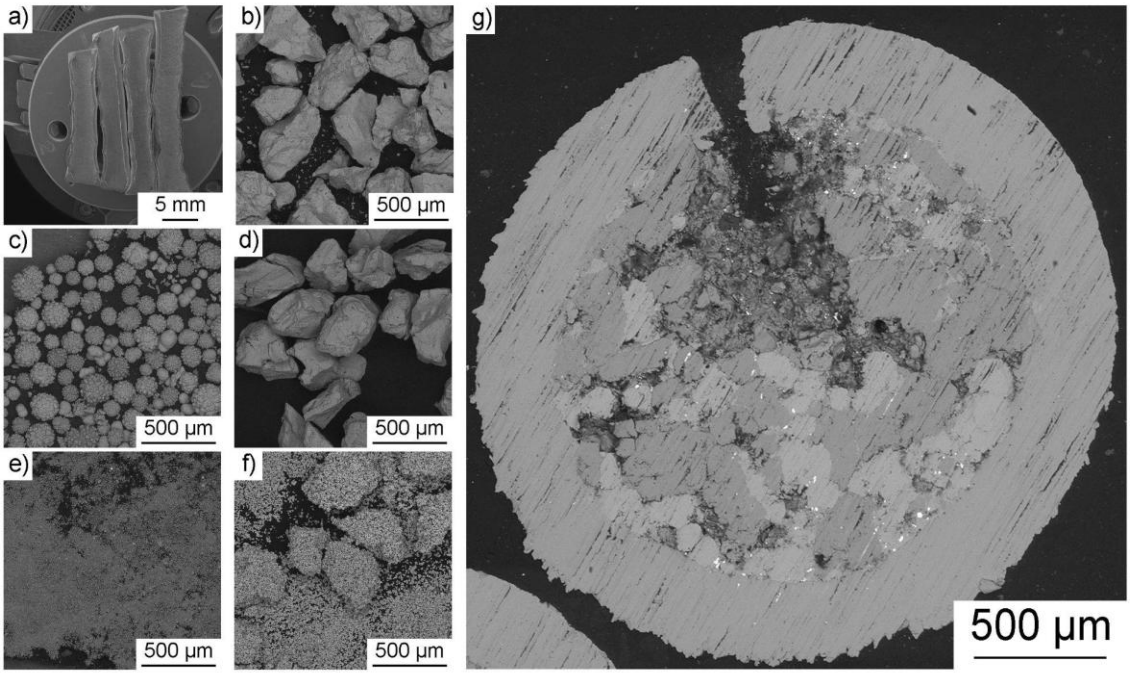


Fig. 2 – Raw materials that were used for production core-wire: a) Fe wire; b) Cr, c) Ni, d) Mn, e) Co, f) W, g) cross-section of crimped wire

The core-wire was filled more than 70 %, **Fig. 3**. It should be mentioned that all powders particles were located in the core wire according to the EDS map analysis, **Fig. 3**. This led to uniform distribution of elements in the wall after deposition.

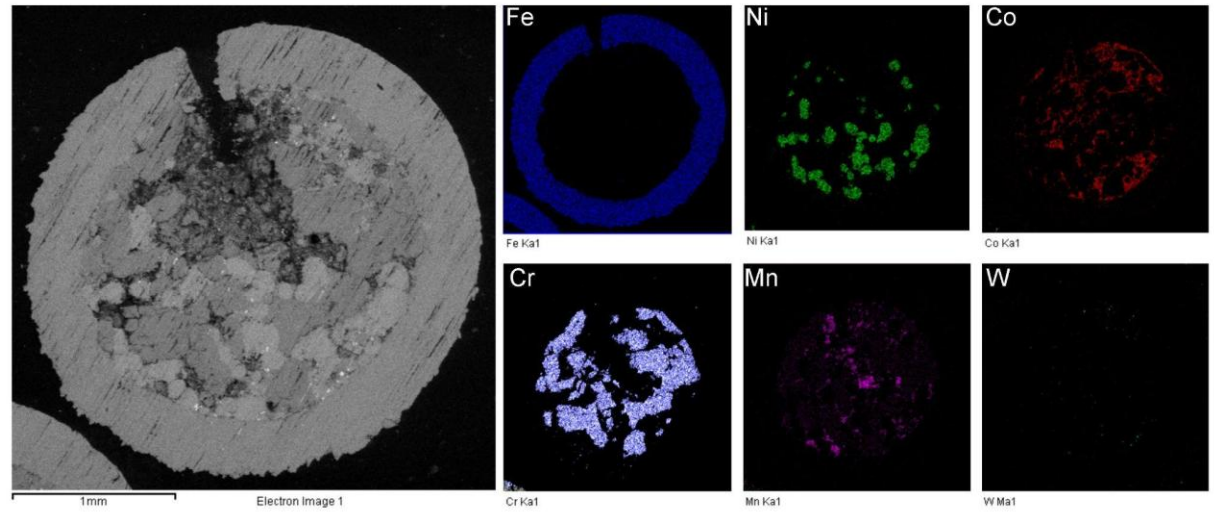


Fig. 3 - Cross section of the core-wire with EDS map elements distribution

The calculation according to the Scheil-Gulliver equation indicates the formation of homogeneous solid solution without precipitation, **Fig. 4 a**. The DSC analysis results of the core wire HEA-W show that melting had a single peak, **Fig. 4 b**. The melting started at 1377°C, the peak of melting was 1408°C and the end of melting at 1414°C. This indicates that all components of the wire melted at the same time as was predicted by calculation, **Fig. 4 a**.

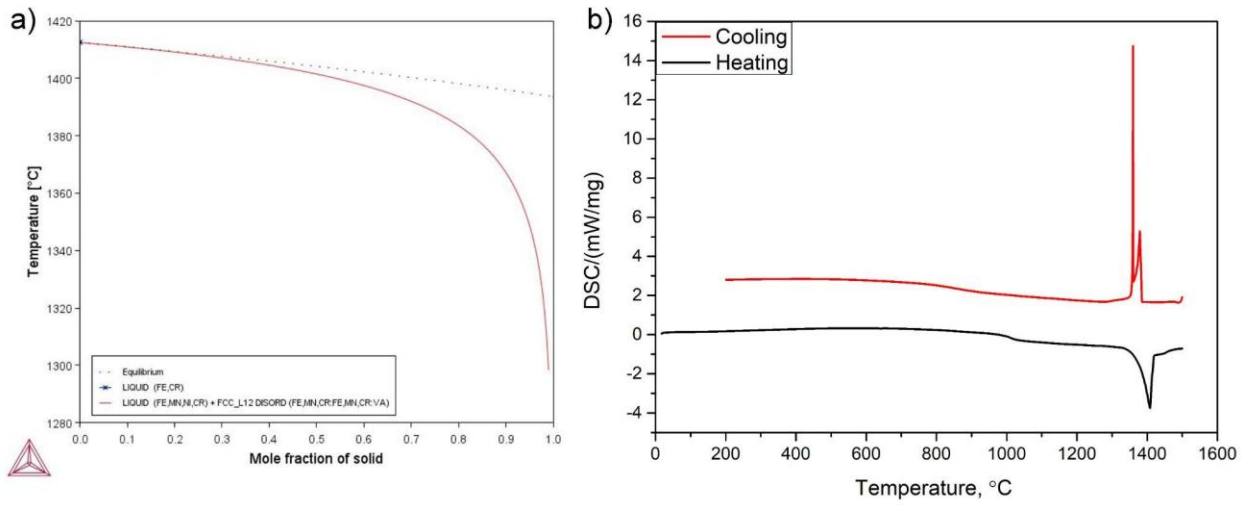


Fig. 4 – Calculation of the Scheil-Gulliver (a), and DSC of the heating and cooling of W-HEA (b)

However, the crystallization process had two peaks, **Fig. 4 b**. The first peak began at 1385°C and the maximum was 1370°C. The highest crystallization peak is observed at 1360°C, and the end of crystallization at 1350°C. The presence of two peaks during cooling indicates that some components crystallize first, and then the others. In our case, the most refractory component is W (3422°C). Therefore, this element acts as a center for crystallization of the HEA, followed by the release of other elements.

XRD of the as-deposed W-HEA is shown on **Fig. 5**. The formation of a single BBC crystalline phase was observed. The lattice constant of W-HEA was 0.3593 nm. It should be noted that the lattice parameter of pure HEA is 0,32205. This indicates that the dissolution of W affects the lattice.

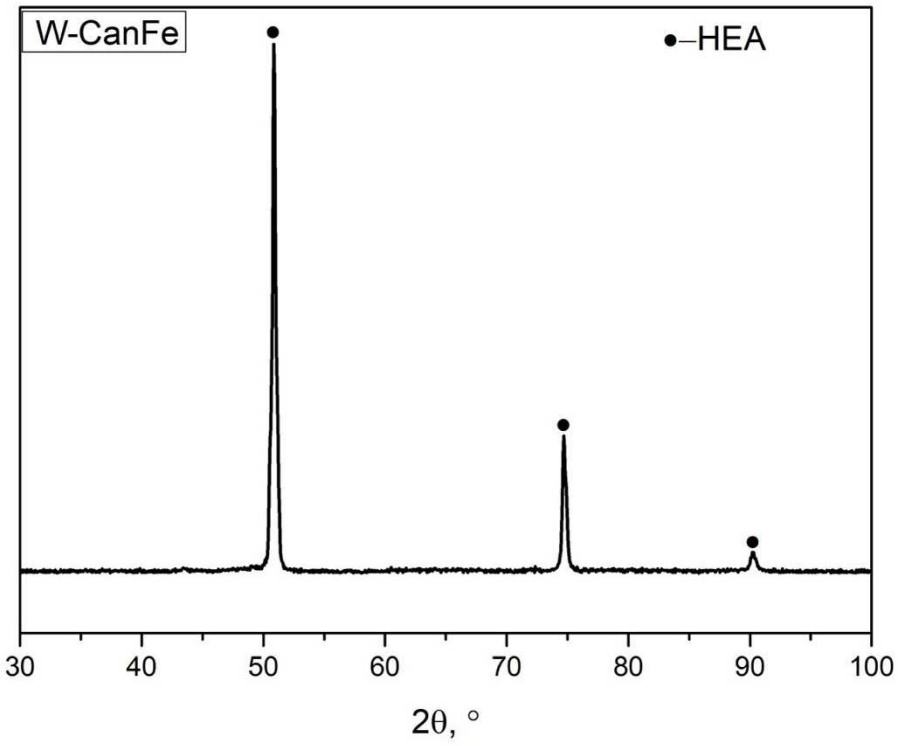


Fig. 5 - XRD of W-HEA after deposition

The microstructure of the W-HEA is shown in **Fig. 6**. The grains in the material have an elongated shape though the all sample, **Fig. 6**. However, the grain size after the deposition depends on the part of the wall, **Fig. 6 a**. In the bottom region of the deposit (Fig. 6a), a finer grain structure with well-defined grain boundaries was observed. The formation of this microstructure is associated with the high cooling rates resulting from efficient heat extraction through the substrate during the initial stages of deposition. Several small pores and inclusions were detected within the matrix; however, their distribution was sparse and no indications of secondary phase formation or pronounced segregation were identified.

The microstructure of the middle part of the wall (Fig. 6b) was characterized by a slight increase in grain size compared with the bottom region. The repeated thermal cycling associated with the deposition of subsequent layers reduced the cooling rate and promoted grain growth. Nevertheless, the alloy retained a homogeneous appearance, and no dendritic morphology or

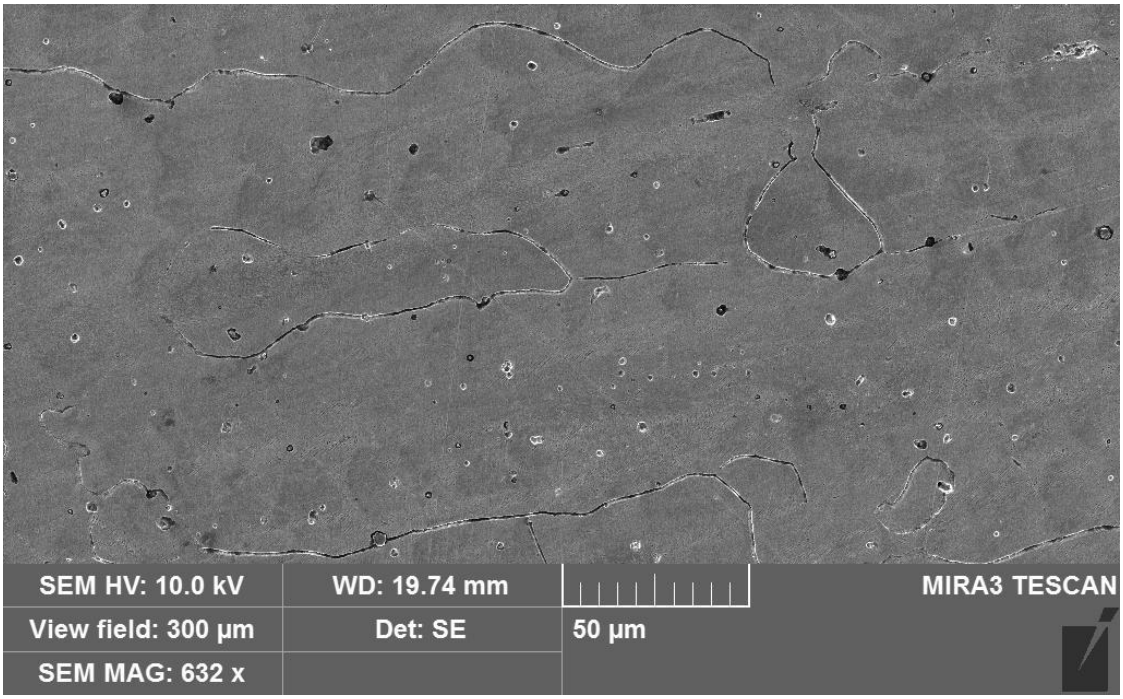
distinct compositional heterogeneities were observed. The density of pores remained low and comparable to that of the lower section of the wall.

Further grain coarsening was detected in the upper part of the deposit (Fig. 6c), where the grains became larger and locally elongated. This behavior can be attributed to the reduced heat dissipation efficiency and prolonged thermal exposure experienced by the upper layers during WAAM processing. Despite these changes, the microstructure remained relatively uniform across the investigated area. No evidence of secondary phase precipitation or segregation zones was found, while the amount and distribution of pores and inclusions did not differ significantly from those observed in the lower regions of the wall.

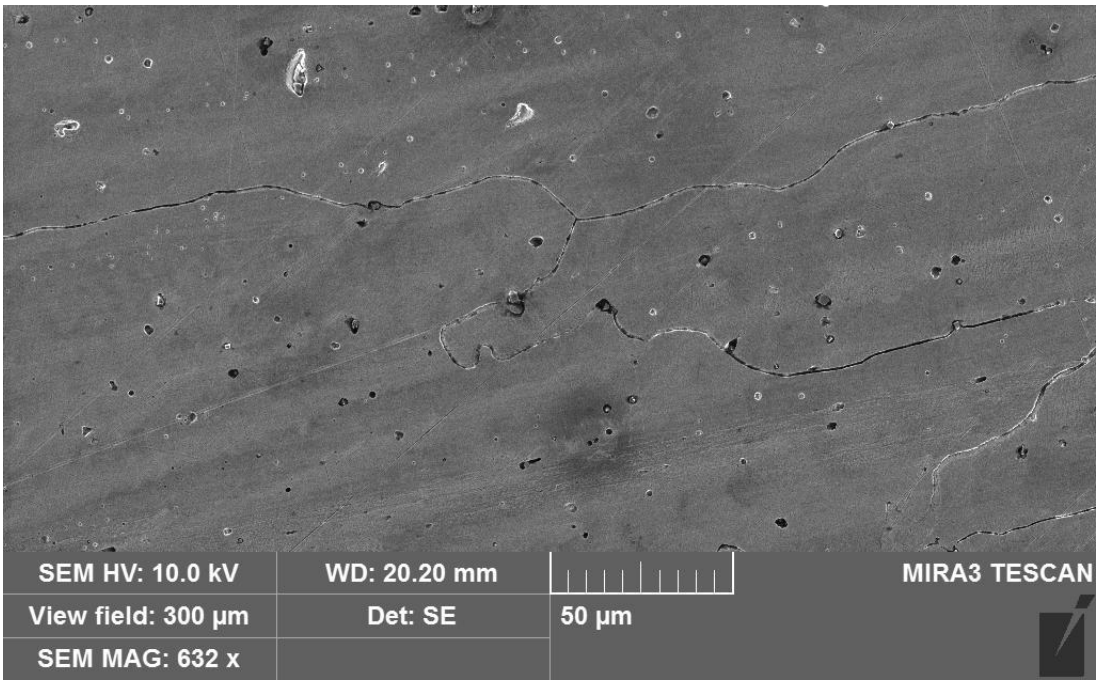
Overall, the W-containing Fe-rich Cantor-type alloy exhibited a structurally homogeneous microstructure along the entire build height. The main microstructural feature associated with the WAAM process was the gradual increase in grain size from the bottom towards the top of the wall, reflecting the evolution of the thermal conditions during deposition. The absence of visible segregation and secondary phases is in good agreement with the XRD and EDS results, confirming the formation of a chemically homogeneous solid-solution matrix.

This grain size in the alloy is primarily dependent on the deposition method. With WAAM technology, the cooling process occurs fast at the substrate, allowing for a fine grain size in the bottom and center part. The slow cooling in the upper part led to large grains in the material due to the low heat transfer.

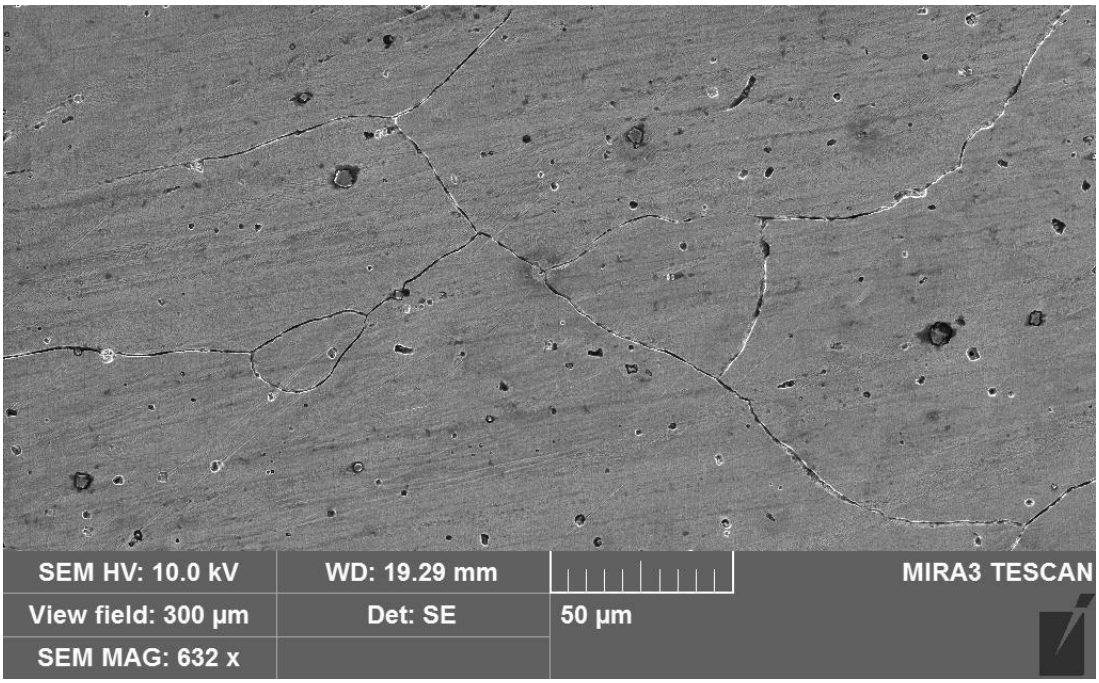
The SEM-EDS map indicates a homogeneous element distribution in the material after WAAM, **Fig. 7**. W has a high absorption capacity, which made it possible to detect a separate peak on the EDS spectrum, **Fig. 7**.


SEM HV: 10.0 kV
WD: 19.74 mm
MIRA3 TESCAN
View field: 300 µm
Det: SE
50 µm
SEM MAG: 632 x

a)


SEM HV: 10.0 kV
WD: 20.20 mm
MIRA3 TESCAN
View field: 300 µm
Det: SE
50 µm
SEM MAG: 632 x

b)



c)

Fig. 6 – Microstructure of W-HEA: a) bottom part of the wall, b) middle part of the wall, c) upper part of the wall

The atomic radius of Fe, Co, Ni, Cr, Mn and W is 140, 135, 135, 140, 140 and 135, respectively. It means that W can be easily dissolved in W-HEA lattice.

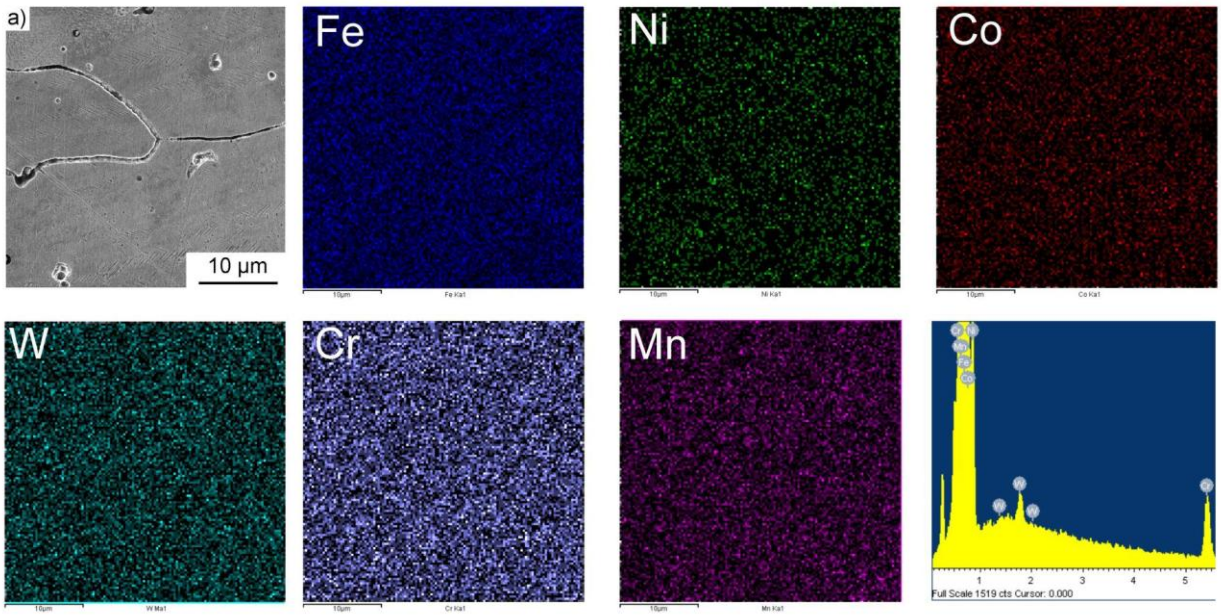


Fig. 7 - SEM and map element distribution at the grain boundaries of W-HEA

Table 1. Chemical composition of the WAAMed W-containing Fe-rich Cantor type HEA

	Cr	Mn	Fe	Co	Ni	W
Top	11.42	8.39	56.39	8.51	14.89	0.40
Middle	11.18	7.19	58.05	8.45	14.66	0.48
Bottom	11.08	7.55	58.75	8.15	14.16	0.32

Overall, the W-containing Fe-rich Cantor-type alloy exhibited a structurally homogeneous microstructure along the entire build height. The main microstructural feature associated with the WAAM process was the gradual increase in grain size from the bottom towards the top of the wall, reflecting the evolution of the thermal conditions during deposition. The absence of visible segregation and secondary phases is in good agreement with the XRD and EDS results, confirming the formation of a chemically homogeneous solid-solution matrix.

EDS analysis performed along the build height revealed only minor variations in chemical composition (Table 1). The Fe content increased slightly towards the bottom region of the wall (56.39–58.75 at.%), whereas Ni, Mn, and W exhibited a tendency for marginal enrichment in the upper layers. Cr and Co concentrations remained nearly constant throughout the deposit. The observed fluctuations did not exceed approximately 2 at.% and no evidence of pronounced macrosegregation was detected, indicating good chemical homogeneity of the W-containing Fe-rich Cantor-type alloy produced by WAAM using metal powder cored wire feedstock.

The engineering stress–strain curves obtained from the middle and upper regions of the deposited wall are presented in Fig. 7. Both specimens exhibited a typical ductile deformation behavior characterized by a short elastic region followed by extensive strain hardening prior to

fracture. The absence of abrupt stress drops indicates stable plastic deformation throughout tensile loading.

The specimen extracted from the **middle part of the wall** demonstrated a slightly higher work-hardening rate during the initial stages of deformation, reaching an ultimate tensile strength of approximately **500 MPa** with a total elongation of about **48%**. In contrast, the specimen obtained from the **upper region** exhibited a comparable ultimate tensile strength but a noticeably higher ductility, with elongation exceeding **55%**.

The difference in deformation behavior can be attributed to the microstructural evolution occurring along the build direction. As demonstrated by SEM observations, the upper layers experienced a lower cooling rate and prolonged thermal exposure, promoting grain coarsening. According to the Hall–Petch relationship, an increase in grain size reduces the resistance to dislocation motion, thereby facilitating plastic deformation. Consequently, the upper region exhibited enhanced ductility while maintaining a strength level comparable to that of the middle section.

The obtained combination of tensile strength and elongation indicates that the W-containing Fe-rich Cantor-type alloy retains a favorable balance between strength and ductility after WAAM processing. Furthermore, the similarity of the tensile curves suggests a relatively homogeneous mechanical response throughout the deposited wall despite the thermal gradients inherent to the WAAM process.

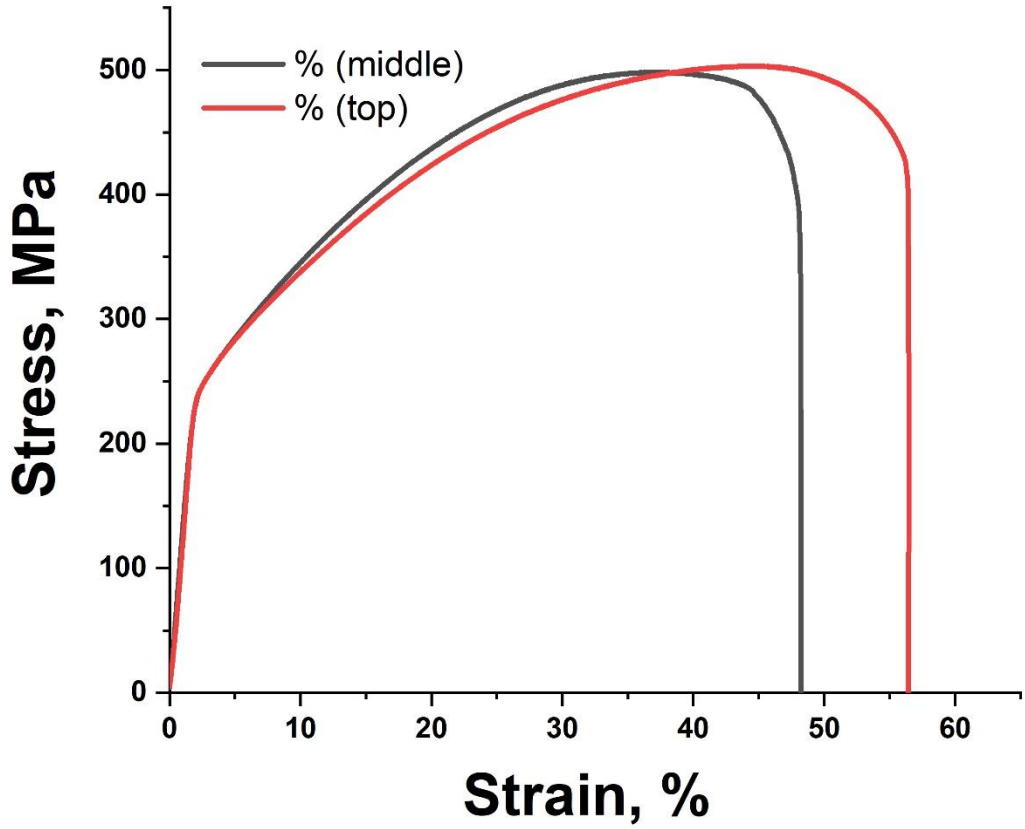


Fig. 7 Engineering stress–strain curves of WAAM W-HEA specimens extracted from the middle (black) and top (red) regions of the deposited wall.

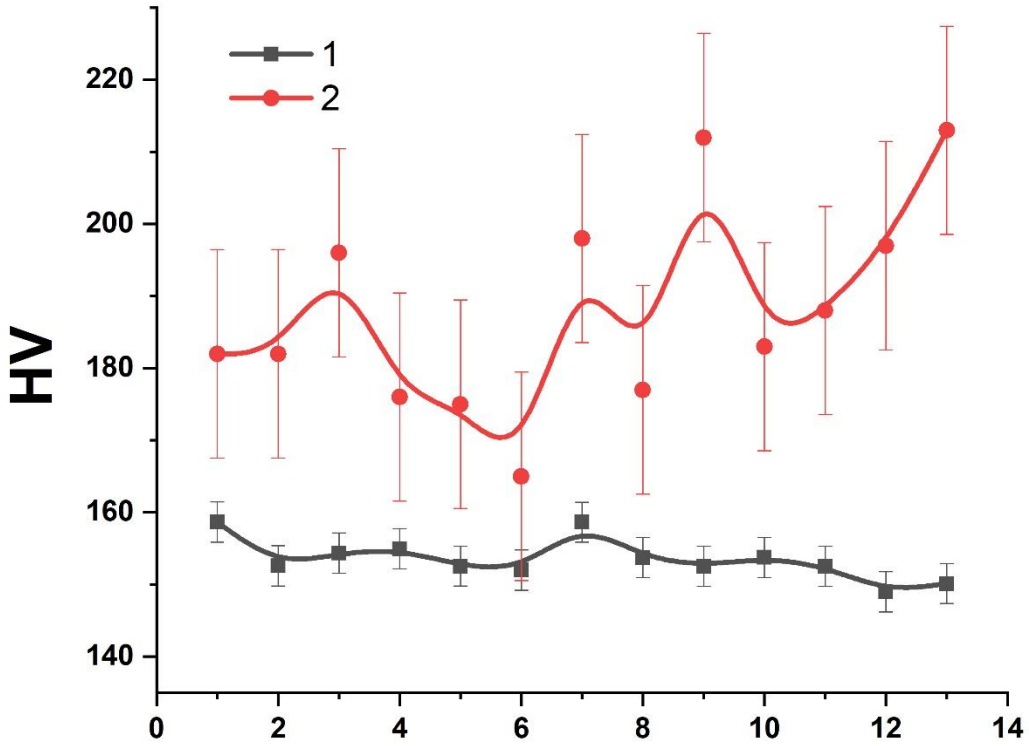


Fig. 8 – Vickers hardness (HV) profiles along the build direction from top to bottom. 1 – Fe-rish Cantor type alloy [17], 2- W-containing Fe-rish Cantor type alloy

The hardness profiles measured along the build direction are shown in Fig. 8. The Fe-rich Cantor alloy (sample 1) exhibited a relatively stable hardness distribution, with values ranging from approximately **149 to 159 HV** and an average hardness of about **154 HV**. Only minor fluctuations were observed, indicating a high degree of microstructural uniformity throughout the deposited wall.

In contrast, the W-containing alloy (sample 2) demonstrated significantly higher hardness values, varying between approximately **165 and 213 HV**. The average hardness increased to about **188 HV**, corresponding to an enhancement of nearly **22%** compared with the W-free alloy.

Despite the larger scatter, the overall hardness level remained consistently higher across the investigated regions.

The increase in hardness can be associated with the solid-solution strengthening effect induced by W addition. Owing to its large atomic radius and high elastic modulus, W promotes local lattice distortion, thereby increasing the resistance to dislocation motion. The increased scatter in hardness values observed in the W-containing alloy may reflect local variations in grain size and the heterogeneous thermal conditions experienced during WAAM deposition.

Interestingly, although W alloying resulted in a pronounced increase in hardness, it did not lead to a corresponding improvement in tensile strength. This observation suggests that the overall mechanical response is governed not only by local strengthening mechanisms but also by the combined influence of grain structure, solidification behavior, and deformation mechanisms operating during tensile loading.

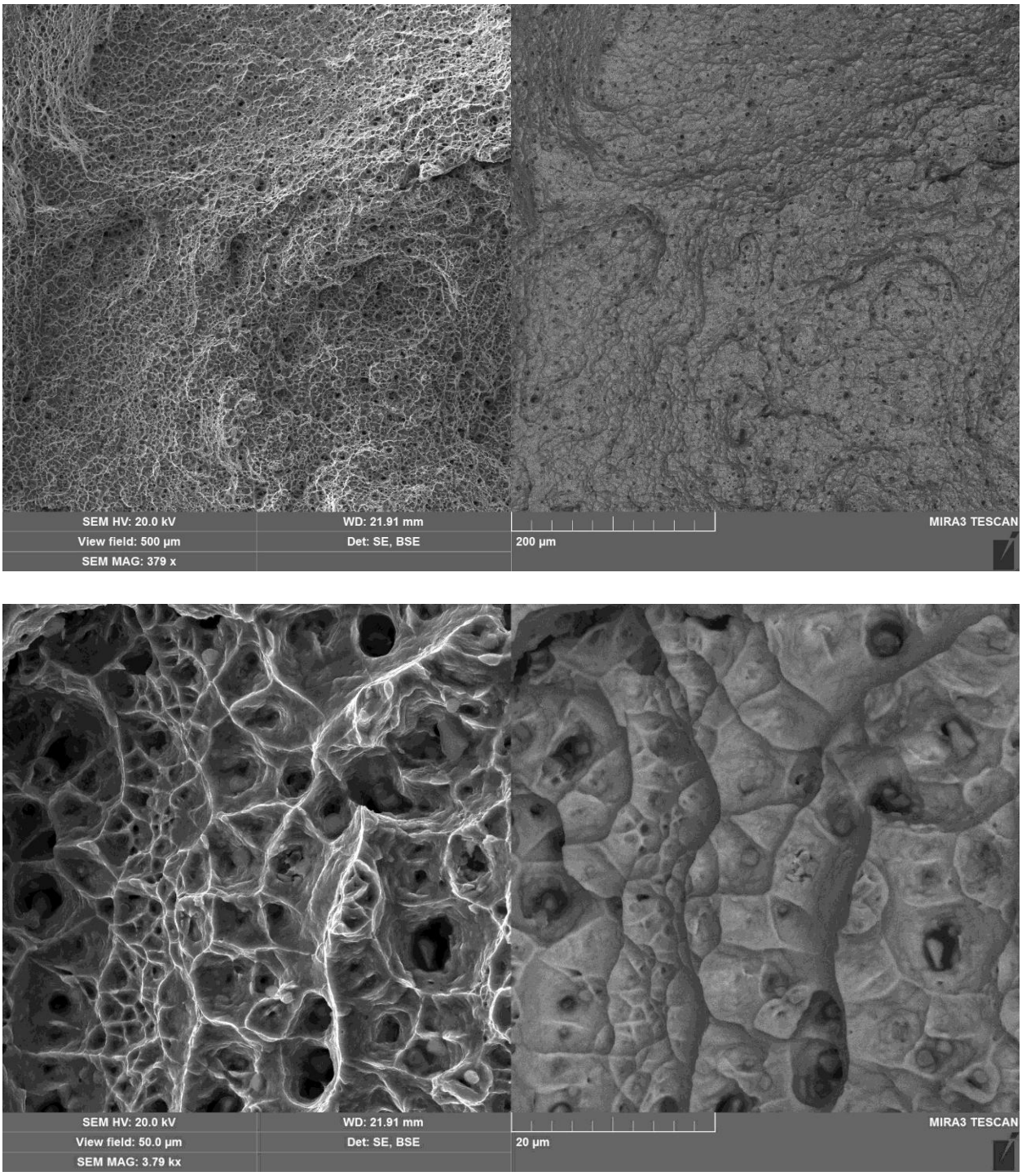


Fig. 9 – SEM fractographs of the tensile fracture surfaces

The fracture surfaces of the tensile specimens are presented in Fig. 9. Regardless of the sampling location, the fracture morphology was predominantly **ductile** in nature and was characterized by the presence of numerous dimples distributed across the fracture surface.

The dimples exhibited variations in size and shape, indicating that fracture proceeded through the nucleation, growth, and coalescence of microvoids during plastic deformation. Fine dimples were frequently observed together with larger voids associated with pores or non-metallic inclusions present in the deposited material. The absence of extensive cleavage facets or intergranular fracture regions suggests that brittle failure mechanisms did not play a significant role in the investigated alloy.

The pronounced plastic deformation evident from the fracture morphology is in good agreement with the tensile test results, which revealed elongation values approaching **50–55%**. These findings confirm that the W-containing Fe-rich Cantor-type alloy preserves substantial ductility after WAAM processing despite the increased hardness associated with W addition.

Overall, the fractographic observations indicate that failure of the deposited alloy occurs predominantly by a **microvoid coalescence mechanism**, reflecting the stable plastic deformation behavior characteristic of compositionally complex Fe-rich Cantor-type alloys.

The combined analysis of tensile properties, hardness measurements, and fracture morphology suggests that W alloying modifies the deformation behavior of the Fe-rich Cantor-type alloy rather than simply increasing its strength. While W addition enhanced hardness through solid-solution strengthening, the simultaneous evolution of the microstructure during WAAM processing, particularly grain coarsening in the upper regions of the wall, contributed to the preservation of excellent ductility. As a result, the deposited alloy exhibited a favorable combination of moderate strength, high plasticity, and homogeneous mechanical performance throughout the build height, which is advantageous for large-scale structural applications produced by WAAM.

4. Conclusions

The present study demonstrated the feasibility of producing a W-alloyed Fe-rich Cantor-type compositionally complex alloy by wire arc additive manufacturing using a metal powder cored wire feedstock. Thermodynamic calculations and DSC analysis revealed that W addition influences the solidification behavior of the alloy, resulting in a multi-stage crystallization process while maintaining a stable solid-solution structure. XRD analysis confirmed the formation of a single BCC phase, whereas SEM-EDS investigations showed a homogeneous distribution of alloying elements without pronounced segregation or secondary phase precipitation. The deposited material exhibited a relatively uniform microstructure throughout the build height, with progressive grain coarsening from the bottom to the top of the wall due to the evolution of thermal conditions during WAAM processing. Mechanical testing revealed a favorable combination of strength and ductility, with ultimate tensile strength reaching approximately 500 MPa and elongation ranging from 48 to 56%, depending on the sampling location. Although W alloying increased the average hardness from approximately 154 HV to 188 HV, no corresponding increase in tensile strength was observed, indicating that the mechanical response is controlled by the interplay between solid-solution strengthening, grain structure evolution, and the thermal history of the deposition process. Fractographic analysis confirmed a predominantly ductile fracture mechanism governed by microvoid nucleation, growth, and coalescence. Overall, the results demonstrate that W alloying provides an effective approach for tailoring the microstructural evolution and local strengthening of Fe-rich Cantor-type alloys fabricated by WAAM, while the use of metal powder cored wire expands the possibilities for compositional design of advanced compositionally complex alloys intended for large-scale structural applications.

Acknowledgements

Autors are deeply acknowledged to Prof. Joao P. Oliveira and Jiajia Shen Department of Materials Science, NOVA School of Science and Technology, Universidade NOVA de Lisboa, for the help with

The work was carried out with the support of the grant "Advanced Science of Ukraine", 174.07/0303 "Creation of new microalloyed high-entropy alloys using methods of additive manufacturing by arc welding"

Statements and Declarations

Conflict of interest: Anatoliy Zavdoveev, Dmytro Vedel, Ji Junwen, Nikša Čatipović, Mykola Skoryk, Andrej Klapatyuk, Sviatoslav Motrunich, Valeriy Pozniakov, Viacheslav Kopylov, Massimo Rogante, Iaroslav Lavrenko declare that they have no conflict of interest.

Author Contributions

Anatoliy Zavdoveev, Dmytro Vedel, Ji Junwen Conceptualization, Methodology; **Anatoliy Zavdoveev, Viacheslav Kopylov** Supervision; **Ji Junwen** Metodology; **Nikša Čatipović, Mykola Skoryk, Andrej Klapatyuk, Sviatoslav Motrunich, Valeriy Pozniakov, Massimo Rogante, Iaroslav Lavrenko**, **Ji Junwen** Data curation, Writing- Original draft preparation. All authors discussed the results and commented on the manuscript.

Availability of Data and Materials

The datasets generated and/or analysed during the current study are not publicly available due to ongoing research but are available from the corresponding author on reasonable request.

5. References

[1] E.P. George, D. Raabe, R.O. Ritchie, High-entropy alloys, Nat. Rev. Mater. 4 (2019) 515–534. https://doi.org/10.1038/s41578-019-0121-4.

[2] S. Chen, Y. Tong, P.K. Liaw, Additive manufacturing of high-entropy alloys: a review, Entropy 20 (2018) 937.

[3] **N. Eißmann, B. Klöden, T. Weißgärber, B. Kieback, High-entropy alloy CoCrFeMnNi produced by powder metallurgy, Powder Metallurgy 60 (2017) 184–197.**

[4] **C.-W. Tsai, Y.-L. Chen, M.-H. Tsai, J.-W. Yeh, T.-T. Shun, S.-K. Chen, Deformation and annealing behaviors of high-entropy alloy Al0.5CoCrCuFeNi, J. Alloys Compd. 486 (2009) 427–435. https://doi.org/https://doi.org/10.1016/j.jallcom.2009.06.182.**

[5] **B. Cantor, I.T.H. Chang, P. Knight, A.J.B. Vincent, Microstructural development in equiatomic multicomponent alloys, Materials Science and Engineering: A 375–377 (2004) 213–218. https://doi.org/https://doi.org/10.1016/j.msea.2003.10.257.**

[6] **Y. Brif, M. Thomas, I. Todd, The use of high-entropy alloys in additive manufacturing, Scr. Mater. 99 (2015). https://doi.org/10.1016/j.scriptamat.2014.11.037.**

[7] **S. Luo, C. Zhao, Y. Su, Q. Liu, Z. Wang, Selective laser melting of dual phase AlCrCuFeNix high entropy alloys: Formability, heterogeneous microstructures and deformation mechanisms, Addit. Manuf. 31 (2020) 100925. https://doi.org/https://doi.org/10.1016/j.addma.2019.100925.**

[8] **H. Dobbelstein, E.L. Gurevich, E.P. George, A. Ostendorf, G. Laplanche, Laser metal deposition of compositionally graded TiZrNbTa refractory high-entropy alloys using elemental powder blends, Addit. Manuf. 25 (2019) 252–262. https://doi.org/https://doi.org/10.1016/j.addma.2018.10.042.**

[9] **S.W. Williams, F. Martina, A.C. Addison, J. Ding, G. Pardal, P. Colegrove, Wire + Arc Additive Manufacturing, Materials Science and Technology 32 (2016) 641–647. https://doi.org/10.1179/1743284715Y.0000000073.**

[10] **W. Yangfan, C. Xizhang, S. Chuanchu, Microstructure and mechanical properties of Inconel 625 fabricated by wire-arc additive manufacturing, Surf. Coat. Technol. 374 (2019) 116–123. https://doi.org/https://doi.org/10.1016/j.surfcoat.2019.05.079.**

[11] **Z. Wang, S. Zimmer-Chevret, F. Léonard, G. Abba, Improvement strategy for the geometric accuracy of bead's beginning and end parts in wire-arc additive manufacturing (WAAM), The International Journal of Advanced Manufacturing Technology (2021). https://doi.org/10.1007/s00170-021-08037-8.**

[12] **B. Saleh, R. Fathi, Y. Tian, N. Radhika, J. Jiang, A. Ma, Fundamentals and advances of wire arc additive manufacturing: materials, process parameters, potential applications, and future trends, Archives of Civil and Mechanical Engineering 23 (2023) 96.**

[13] **C.R. Cunningham, S. Wikshåland, F. Xu, N. Kemakolam, A. Shokrani, V. Dhokia, S.T. Newman, Cost Modelling and Sensitivity Analysis of Wire and Arc Additive**

Manufacturing, Procedia Manuf. 11 (2017) 650–657. https://doi.org/https://doi.org/10.1016/j.promfg.2017.07.163.

[14] V. Votruba, I. Diviš, L. Pilsová, P. Zeman, L. Beránek, J. Horváth, J. Smolík, Experimental investigation of CMT discontinuous wire arc additive manufacturing of Inconel 625, The International Journal of Advanced Manufacturing Technology 122 (2022) 711–727. https://doi.org/10.1007/s00170-022-09878-7.

[15] A. Zavdoveev, V. Pozniakov, T. Baudin, H.S. Kim, I. Klochkov, S. Motrunich, M. Heaton, P. Aquier, M. Rogante, A. Denisenko, A. Gajvoronskiy, M. Skoryk, Optimization of the pulsed arc welding parameters for wire arc additive manufacturing in austenitic steel applications, The International Journal of Advanced Manufacturing Technology 119 (2022) 5175–5193. https://doi.org/10.1007/s00170-022-08704-4.

[16] J. Guo, Y. Zhou, C. Liu, Q. Wu, X. Chen, J. Lu, Wire Arc Additive Manufacturing of AZ31 Magnesium Alloy: Grain Refinement by Adjusting Pulse Frequency, Materials 9 (2016). https://doi.org/10.3390/ma9100823.

[17] A. Zavdoveev, A. Klapatyuk, T. Baudin, E. MacDonald, D. Mohan, J. Oliveira, A. Gajvoronskiy, V. Poznyakov, H.S. Kim, F. Brisset, M. Khokhlov, M. Heaton, M. Rogante, M. Skoryk, D. Vedel, R. Kozin, I. Klochkov, S. Motrunich, Non-equimolar Cantor high entropy alloy fabrication using metal powder cored wire arc additive manufacturing, Additive Manufacturing Letters (2023) 100124. https://doi.org/https://doi.org/10.1016/j.addlet.2023.100124.

[18] A. Zavdoveev, H.S. Kim, Y.-U. Heo, T. Baudin, P. Cortes, F. Brisset, D.-H. Kim, D. Vedel, A. Klapatyuk, A. Gajvoronskiy, V. Poznyakov, E. Pashinska, S. Motrunich, Microstructure and properties of HEA fabricated through metal powder wire arc additive manufacturing, Mater. Lett. 357 (2024) 135726. https://doi.org/https://doi.org/10.1016/j.matlet.2023.135726.

[19] A. Zavdoveev, T. Baudin, F. Brisset, M. Speicher, A. Klapatyuk, A. Gaivoronskiy, V. Poznyakov, D. Vedel, I. Klochkov, J. Junwen, High hardness Ta doped eutectic high entropy alloy by wire arc additive manufacturing, The International Journal of Advanced Manufacturing Technology 138 (2025) 1251–1258.